Proceedings of Ninth World Conference on Earthquake Engineering
August 2-9, 1988, Tokyo-Kyoto, JAPAN (Vol.V)

7-9-6

CONTROL OF EARTHQUAKE ENERGY PARTITIONING IN BASE ISOLATED AND DYNAMICALLY DAMPED STRUCTURES

Hirokazu IEMURA

Associate Professor, Earthquake Engineering Laboratory
Dept. of Civil Eng., Kyoto University, Kyoto 606, JAPAN

SUMMARY

New Earthquake energy spectra are proposed for practical design procedures using energy concepts. The spectra show intergrated earthquake input energy of an unit mass with given natural period and damping ratio. The total input energy and its partitioning in complex structures are evaluated with an example application of modal analysis and the proposed spectra. Numerical simulations are carried out for inelastic structures to show the earthquake energy partitioning in time and in space. Effects of inelastic restoring forces of base isolators and of tuned mass dampers subjected to earthquake ground motions are evaluated for practical design purposes.

INTRODUCTION

The earthquake input energy and its partioning in structures have been studied to develop a new approach for earthquake damage assessment. The earthquake input energy which includes both intensity and duration of ground motion is expected to represent earthquake damage more accurately than the conventional instataneous maximum responses. In the first part of this study, the new earthquake energy spectra are proposed for practical design procedures. The spectra show intergrated earthquake input energy of a unit mass with given natural period and damping ratio. Mathematical formulation is presented for evaluation of the total input energy and its partitioning in complex structures by applying the modal analysis and the proposed energy spectra. In the second part, numerical simulations are carried out for inelastic structures to show earthquake energy partitioning in time and in space. Effects of inelastic restoring forces of base isolators and of tuned mass dampers, subjected to earthquake ground motions, are evaluated for practical design purposes.

EARTHQUAKE INPUT ENERGY SPECTRA

Equation of motion of a single-degree-of-freedom inelastic structure with mass m, damping coefficient c and hysteritic restoring force F(x), subjected to earthquake ground acceleration $\ddot{Z}$ is

$$m\ddot{x} + C\dot{x} + F(x) = -m\ddot{z} \qquad (1)$$

Multiplying by $dx(=\dot{x}dt)$ and integrating each term of Eq.(1) for duration of earthquake ground motion $(0\sim t_0)$, there follows,

$$\frac{1}{2} m \dot{x}^2(t_0) + \int_0^{t_0} C \dot{x}^2 \, dt + \int_0^{t_0} F(x) \dot{x} \, dt = - \int_0^{t_0} m \ddot{x}(t) \ddot{z} \, dt \qquad (2)$$

The first term on the left hand side Eq.(2) represents kinetic energy of mass at the time t_0, second term is the energy absorbed by viscous damping during vibration, and the third term includes both accumulated and dissipated energies by the hysteresis loops of the restoring force up to the time t_0. Right hand side of Eq.(2) shows the earthquake input energy to a structure from the time 0 to t_0.

Partitioning of the earthquake energy in time domain, represented by Eq.(2), is shown in Figs. 1 and 2 for linear and inelastic structure, respectively. NS component of El Centro accelerogrum (1940), and bilinear hysteresis loops are used for numerical calculation. Although the earthquake input energy is similar, its partitioning in linear and in inelastic structure is quite different. The kinetic energy W_K and the potential energy W_E are much smaller due to the hysteretic energy absorption W_H.

The earthquake input energy to a linear SDOF system with an unit mass, at the end of excitation, is a function of natural period and of damping factor. As for conventional response spectra, it is named as "the earthquake input response spectra" and is plotted in Fig. 3(a). It is found that larger damping gives smother spectra which are not always smaller than spectra with lower damping. This is because a structure with larger damping receives broader frequency band of excitation. The equivalent velocity response spectrum, Veq, calculated from the eqrthquake input energy spectra E, defined by Veq = $\sqrt{2E}$, is plotted in Fig. 3(b). The equivalent acceleration response spectrum, Aeq, defined by Aeq = $W_0 \cdot$ Veq is plotted in Fig. 3(c) and is close to the conventional acceleration response spectra with low damping, shown in Fig.3(d).

ENERGY PARTITIONING IN COMPLEX STRUCTURES

When we consider a MDOF structure as shown in Fig. 4, the energy partionting in it is written as

$$\sum_i \left(\frac{1}{2} m_i \dot{x}_i^2 \right) + \sum_i \int_0^{t_0} C_i \dot{y}_i^2 \, dt + \sum_i \int_0^{t_0} F_i \dot{y}_i \, dt = \sum_i \int_0^{t_0} (-m_i \ddot{x}_i \ddot{z}) \, dt \qquad (3)$$

where i denotes i-th mass or i-th interstory. Eq.(3) can be written also as

$$\sum_i W_{Ki} + \sum_i W_{Ci} + \sum_i W_{Ei} + \sum_i W_{Hi} = \sum_i E_i \qquad (4)$$

At the end of response, kinetic and potential energies vanish, and Eq.(4) becomes

$$\sum_i W_{Ci} + \sum_i W_{Hi} = \sum_i E_i \qquad (5)$$

Estimation of Earthquake Input Energy to Linear MDOF Structures

Using the modal analysis and the proposed earthquake input energy spectra, the total earthquake input energy to a linear MDOF structure can be described by

$$\sum_i \int_0^{t_0} (-m_i \ddot{x}_i \ddot{z}) \, dt = \sum_i \left\{ -m_i \int_0^{t_0} \left(\sum_s \phi_{is} \dot{y}_s \right) \ddot{z} \right\} dt = \sum_i m_i \left(\sum_s \phi_{is} E_s \right) \qquad (6)$$

where E_s is the earthquake input energy in s-th mode. E_s can be found from the proposed energy spectra. When there is no modal coupling, the earthquake input energy estimated by Eq.(6) agrees perfectly with the results of step-by-step numerical calculation. Hence, the control of earthquake input energy and its partitioning can be carried out with relatively simple procedures.

Simulation of Energy Partitooning in Base Isolated and Dynamically Damped Structures

The partitioning of earthquake energy in base isolated and dynamically damped structures with bi-linear inelastic restoring force has been simulated numerically. The three models, with mass and stiffness distributions shown in Table 1 are used for the simulation. The models 1, 2, and 3 have been chosen to illustrate regular, base isolated, and dynamically damped structures, respectively. NS component of El Centro accelerogram is used as input ground motion.

Spatial Energy Partitioning

Spatial partitioning of earthquake energy for model 1 is plotted in Fig. 6 showing dependence of the results on damping ratio. $E_i/\Sigma E_i$, $W_{ci}/\Sigma E_i$, and $W_{Hi}/\Sigma E_i$ denote earthquake input energy to the i-th mass, absorbed energy by viscous damping, and by hysteresis loops at i-th interstory, respectively, all normalized by the total input energy. It is found that sifnificant part of the available earthquake energy goes into the first story mass and consequently the first interstory absorbs the largest amount of energy. It is interesting to notice that more uniform spatial partitioning of the input energy is found with the higher damping ratio. This is because the higher shear force is transmitted to the upper stories by larger damping.

In Fig.7, the spatial partitioning for the base isolated structure (model 2) is illustrated and corresponding hysteresis loops of all interstory restoring force and displacement are plotted in Fig.8. In Fig.7, it is found that the earthquake energy goes into upper stories with relatively uniform distribution. However, almost all of it is absorbed by the basement story with viscous and hysteretic damping. The relative displacement of the basement story is five times larger than that of the upper stories. Thus, it is important for design of base isolators to have enough capacity not only for displacement, but also for energy absorption.

In Figs.9. and 10, the spatial partitioning and the corresponding hysteresis loops for the dynamically damped structure (model 3) are shown. It is interesting to notice in this example that the tuned mass has no earthquake input energy, but large amount of energy is absorbed at the interstory between the tuned mass and the structure. This indicates that the tuned mass is standing still in space and working to suppress dynamic response of the structure.

Total Earthquake Input energy

The total earthquake input energy ΣE_i, the net input energy to structures TE (which is calculated by subtracting the absorbed energy by the isolaters or by the tuned mass dampers from ΣE_i) and the absorbed energy by the hysteresis loops TW_H are shown for 3 models in Table 2. From the results of model 1, it is found that the total input energy is increased with higher damping ratio, but TW_H which is a parameter for structural damage is decreased. In model 2, the total input energy is reduced due to long first natural period of base isolated structures. In addition to this, the net input energy and the TW_H in structures are reduced significantly, because most of the total input energy is absorbed by the isolators. In model 3, the total input energy is increased due to additional mass of the tuned mass dampers, and values of TW_H are similar to those of regular type structures. These results indicate that structural damage can be reduced more effectively by the base isolators than by the tuned mass dampers.

CONCLUSIONS

To develope earthquake energy based design concept, the new earthquake energy spectra are proposed. Analytical control of partitioning the earthquake energy

in base isolated and dynamically damped structures has become possible with use of the spectra and modal analysis. Effects of inelastic behavior of isolators and of dampers are evaluated from numerical simulations. Appropriately designed isolators are found not only to suppress the earthquake input energy but also to absorb most of it, thus, reducing the structural damage significantly.

ACKNOWLEDGEMENTS

The author wants to express his sincere thanks to Professor Yoshikazu Yamada, of Kyoto University, Professor M. D. Trifunac of University of Southern California, and to the graduate student Mr. Y. Iwasaki of Kyoto University for their discussions, reviewing, and numerical computation for this study.

REFERENCES

1. Kato, B and Akiyama, H.: Energy Input and Damages in Structures subjected to severe Earthquakes, Proc. of AIJ, No. 235, 9-18, (1975 in Japanese)
2. Ohno, T., Nishioka, T. and Fujino, Y.: Quantative Estimation of Plastic Energy absorbed in Structures subjected to Seismic Excitation, Proc. of JSCE No. 333, 91-99, May, (1983 in Japanese)
3. Iemura, H.: Hybrid Experiments on Earthquake Failure Criteria of Reinforced Concrete Structures, Proceedings of the Eighth WCEE, Vol. VI, 103-110, (1984)

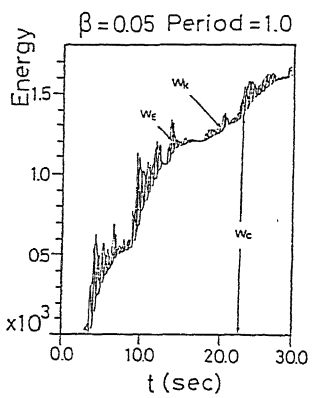

Fig.1 Input Earthquake Energy to a Linear Structure

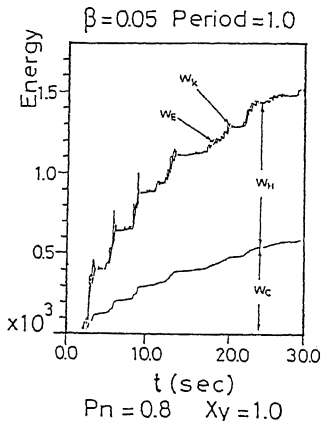

Fig.2 Input Earthquake Energy to an Inelastic Structure

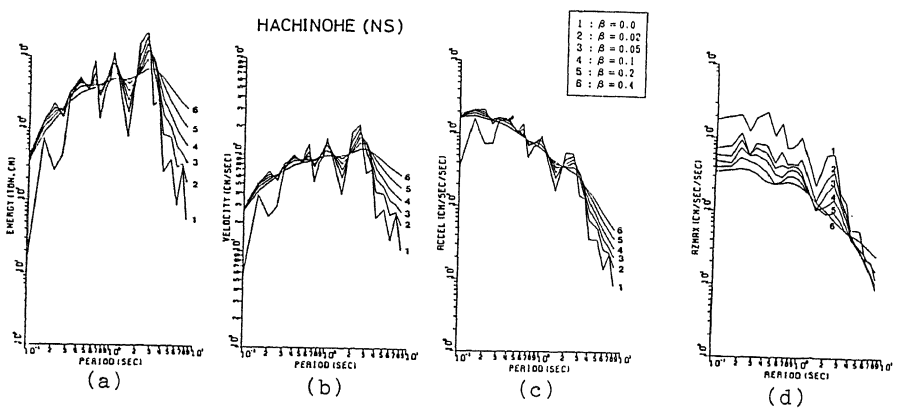

Fig.3 Earthquake Energy Based Spectra and Conventional Response Spectra

Table 1 Mass and Stiffness of Each Model

	No	B	1	2	3	4	5	6
Model 1	k (ton/cm)		250.0	250.0	250.0	250.0	250.0	
	m (ton)		4.0	4.0	4.0	4.0	4.0	
Model 2	k (ton/cm)	100.0	250.0	250.0	250.0	250.0	250.0	
	m (ton)	5.0	4.0	4.0	4.0	4.0	4.0	
Model 3	k (ton/cm)		250.0	250.0	250.0	250.0	250.0	10.0
	m (ton)		4.0	4.0	4.0	4.0	4.0	2.0

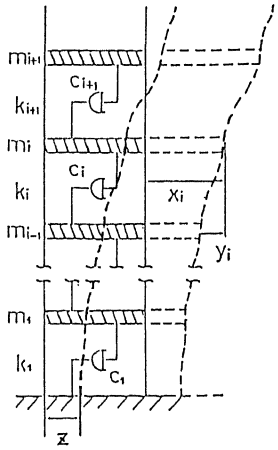

Fig.4
Multi DOF Structural Model

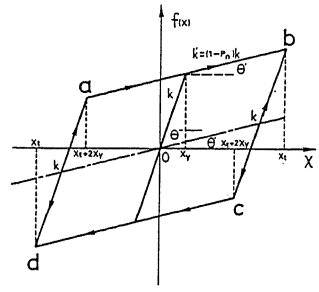

Fig.5 Bi-linear Inelastic Restoring Force

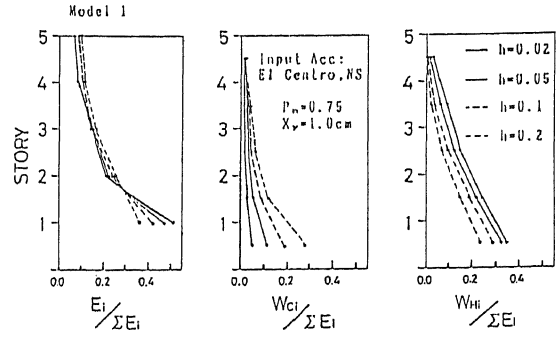

Fig.6 Space Partitioning of Earthquake Energy Regular Structural Model (Model 1)

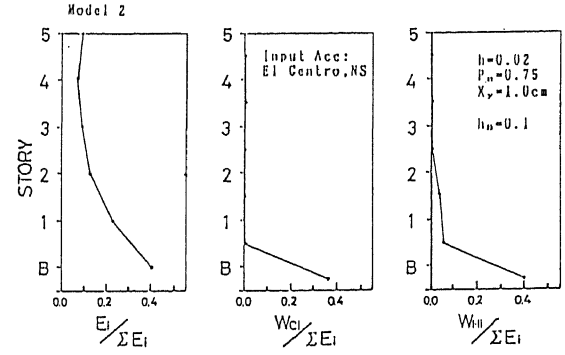

Fig.7 Space Partitioning of Earthquake Energy Base Isolated Structural Model (Model 2)

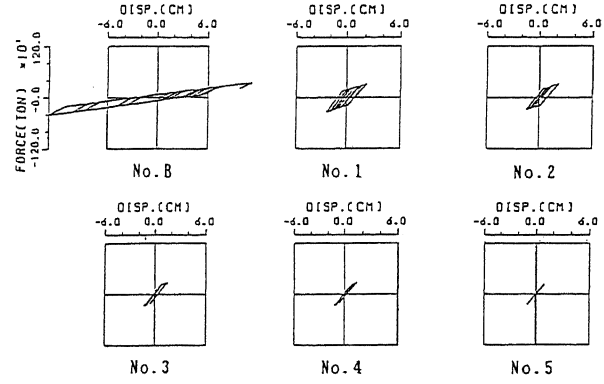

Fig.8 Hysteresis Loop of Each Story of a Base Isolated Structural Model (Model 2)

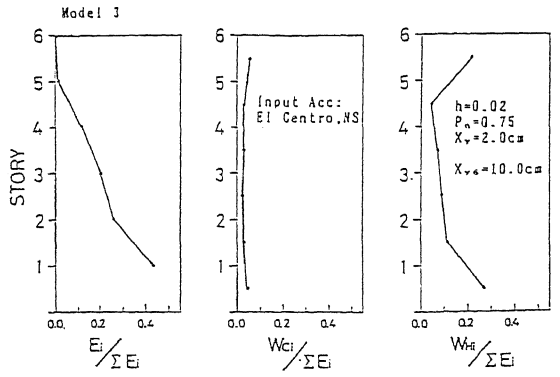

Fig.9 Space Partitioning of Earthquake Energy Dynamically Damped Structural Model (Model 3)

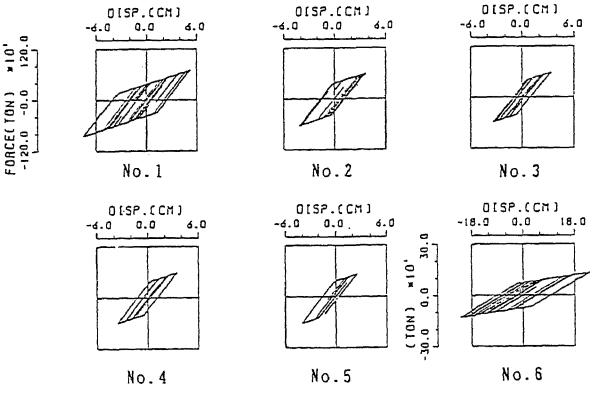

Fig.10 Hysteresis Loop of Each Story of a Dynamically Damped Structural Model (Model 3)

Table 2 Total Energy

Model 1

h	x_y (cm)	P_n	ΣE_i (ton·cm)	TE (ton·cm)	TW_H (ton·cm)
0.02	1.0	0.75	36,161.3	—	31,095.2
0.05	1.0	0.75	36,604.1	—	26,943.0
0.10	1.0	0.75	39,669.3	—	24,309.5
0.2	1.0	0.75	43,634.1	—	20,406.7

Model 2

h_n	x_{yn} (cm)	P_{nn}	ΣE_i (ton·cm)	TE (ton·cm)	TW_H (ton·cm)
0.1	1.0	0.75	23,667.0	5,429.6	2,807.2
0.02	1.0	0.75	19,626.6	6,065.7	2,696.0
0.1	0.5	0.75	21,131.7	4,310.8	1,637.5
0.1	2.0	0.75	26,716.9	8,891.1	6,632.5
0.1	1.0	0.60	26,448.7	10,784.0	7,606.7
0.1	1.0	0.85	23,131.0	3,024.2	1,066.6

Model 3

h_6	x_{y6} (cm)	P_{n6}	ΣE_i (ton·cm)	TE (ton·cm)	TW_H (ton·cm)
0.02	10.0	0.75	45,737.2	33,727.7	26,032.7
0.1	10.0	0.75	46,246.6	33,046.0	25,817.6
0.1	∞	—	44,931.3	32,916.0	25,369.3
0.1	6.0	0.75	50,123.0	36,667.8	29,357.0